Polymer Chemistry

ROYAL SOCIETY OF CHEMISTRY

PAPER

View Article Online
View Journal | View Issue

Cite this: *Polym. Chem.*, 2024, **15**, 2177

Fluorescent poly(β-amino ester)s containing aza-BODIPYs as theranostic agents for bioimaging and photodynamic therapy†

Seyma Sari,[a] Sena Ünver,[b] Timucin Avsar,[c] Şennur Özçelik,[d] Turker Kilic[e] and Muhammet U. Kahveci *[d]

Received 22nd March 2024,
Accepted 29th April 2024

DOI: 10.1039/d4py00318g

rsc.li/polymers

Photodynamic therapy (PDT) as a promising approach in cancer treatment has garnered significant attention due to its minimal invasiveness and low toxicity, as well as its ability to avoid side effects and facilitate combination therapies. The photosensitizer (PS) is the key component of PDT and can be employed in the diagnosis or visualization of cells. Herein, a water-dispersible, biodegradable and fluorescent poly (β-amino ester) (PBAE) based PS was developed for efficient PDT and imaging. The PBAE was specifically designed and synthesized to incorporate fluorescent groups, such as aza-BODIPY, and water soluble poly (ethylene glycol) segments into the polymer backbone by aza-Michael addition-based poly-condensation polymerization. Subsequently, the amine-end functionalized PBAEs with different aza-BODIPY contents (3.6 and 7.2 mol%) were end-capped with folic acid to increase the cancer-cell-targeting potential of the polymers. The polymeric PSs were then tested on brain tumor (U87-MG), cervical tumor (HeLa) and healthy (HUVEC) cell lines for the dual modality of imaging and PDT. The polymeric PSs demonstrated significant anti-cancer potential as evaluated *via* reactive oxygen species generation, photocytotoxicity, colony formation and cell invasion assays.

Introduction

Cancer is one of the major health problems causing a high number of deaths, with almost 10 million deaths and 19.3 million new cancer cases worldwide in 2020.[1] Surgery, chemotherapy, and radiation are the most widely employed approaches for its treatment. However, these traditional approaches have serious drawbacks such as very harmful side effects since healthy and cancerous cells cannot be easily distinguished.[2] To overcome such shortcomings, targeted delivery of therapeutics, localized therapy and novel modes of therapy such as hyperthermia and photodynamic therapy (PDT) have been developed. As PDT is minimally invasive, minimally toxic, causes no side effects, and allows for combination therapies, it has attracted tremendous interest.[3,4] The most outstanding advantage of PDT is its benign nature leading to a more pleasant treatment. This promising technique has three key constituents: light, a photosensitizer (PS) and molecular oxygen. A PS is non-toxic without light, but upon light irradiation, it generates reactive oxygen species (ROS) such as $^1O_2$, O^{2-} and $^{\bullet}OH$ that attack biological molecules and ultimately cause the inhibition of proliferation of target (cancer) cells.[2,3,5] PDT reduces adverse side effects and complications by providing temporal and spatial control during the treatment, compared to the traditional methods. Recently, great efforts have been made to provide PDT theranostic treatment with a dual modality, that is, diagnostic and therapeutic.[6–10]

The success of PDT mainly depends on the effectiveness of the PS in terms of transfer and translation of light energy into a chemical reaction. Photofrin, a mixture of oligomeric porphyrin units, is the first approved PS by the Food and Drug Administration (FDA) and opened a new horizon in cancer treatment;[11] however, even it exhibited certain drawbacks.[12] Since then, many PSs have been developed to ensure the fundamental needs for PDT such as nontoxicity, photostability, selectivity, targetability, suitable elimination profile, water solubility and reliable photochemical properties.[13–15] The macrocyclic structure of most PSs is associated with an important disadvantage: low/lack of water solubility, caused by their strong tendency for aggregation. In addition, their tiresome synthesis and modification of

[a]*Istanbul Technical University, Graduate School, Chemistry Programme, Maslak, Sariyer, 34467 Istanbul, Türkiye*
[b]*Health Science Institute, Bahcesehir University, Goztepe, 34734 Istanbul, Türkiye*
[c]*Department of Medical Biology, School of Medicine, Bahcesehir University, Goztepe, 34734 Istanbul, Türkiye*
[d]*Istanbul Technical University, Faculty of Science and Letters, Department of Chemistry, Maslak, Sariyer, 34467 Istanbul, Türkiye. E-mail: kahvecimuh@itu.edu.tr*
[e]*Department of Neurosurgery, School of Medicine, Bahcesehir University, Goztepe, 34734 Istanbul, Türkiye*

† Electronic supplementary information (ESI) available: Reaction schemes, NMR, FT-IR, UV-Vis and fluorescence spectra and microscopy images. See DOI: https://doi.org/10.1039/d4py00318g

their photophysical properties are troublesome and time consuming.[15] Furthermore, they show low selectivity for cancerous cells over healthy ones.[16] Therefore, recently great efforts have been made to construct PSs with higher selectivities and efficiencies for both PDT and imaging.[17,18]

Boron dipyrromethenes (BODIPYs) and boron azadipyrromethenes (aza-BODIPYs) are an important class of dyes employed in many advanced applications. In addition to their typical advantages such as low dark-toxicity, high generation of singlet oxygen, high extinction coefficients at long wavelengths, and resistance to photobleaching, aza-BODIPYs bring superior photophysical properties owing to a meso-nitrogen atom between two pyrroles.[19,20] Their excitation ($\lambda_{exc.}$ = 650–675 nm) and fluorescence emission wavelengths ($\lambda_{emis.}$ = 700–900 nm) are red-shifted to longer wavelengths (near infrared, NIR) compared to those of classical BODIPYs.[21] These wavelengths fall in the "therapeutic window" that enables deep tissue penetration and higher contrast. Therefore, aza-BODIPYs are considered promising PSs for dual modality involving fluorescence imaging and treatment,[22,23] and they fulfill the features of an ideal fluorophore.[24] However, the planar and rigid nature of the aza-BODIPY core causes the aggregation phenomenon and poor water solubility, which limits the implementation of this valuable dye in biomedical applications such as bioimaging and PDT.[24,25] Structural modifications such as the incorporation of water soluble groups, such as ammonium[24,26] and sulfonate[21,27,28] groups, or conjugation of water soluble polymers[29,30] or oligomers[31] are the most widely used methods to circumvent this serious drawback. Alternatively, hydrophobic aza-BODIPY molecules are encapsulated into polymeric micelles, and, thus, dispersed in aqueous media.[32–34]

Fluorescent polymers are an important class of dyes utilized in PDT, diagnosis and bioimaging, due to their enhanced photostability, multi-functionality, tunable photochemical properties, improved extinction coefficients and biocompatibility.[35,36] In addition to these properties, when compared to their small-molecule counterparts, polymeric PSs exhibit some other advantages including a higher absorption cross-section and ease of functionalization.[37] Moreover, polymeric PSs can allow targeted delivery of therapeutics into a tumor environment by achieving a discrimination between the cancerous and healthy cells/tissues. Nano-sized polymeric particles are an important class of materials for passive tumor targeting due to their enhanced permeability and retention (EPR) effect.[38] In addition, such polymeric materials can be specifically designed to carry various targeting molecules such as antibodies against tumor markers, aptamers, carbohydrates, vitamins and peptides or ligands of overexpressed receptors.[39] FA is a widely utilized targeting ligand since FA receptors are overexpressed in many cancer cell lines.[40–42] For instance, brain tissues express excess FA receptors which may allow delivery vehicles to pass the blood–brain barrier for treatment of gliomas.[40] Human cervical cancer cells (HeLa)[43] also overexpress FA receptors and can be targeted by FA-containing delivery systems.

Recently, much effort has been made for the development of water-soluble/dispersible fluorescent polymers for PDT, diagnosis and bioimaging.[44–47] In addition, the non-biodegradability of conjugated polymers leads to prolonged metabolic time causing long-term cytotoxicity and undesirable side effects *in vivo*. Thus, the development of biodegradable fluorescent polymers is important and highly desirable for future translational research.[48–50] Poly(β-amino ester)s (PBAEs) are highly biodegradable polymers and can be utilized for the construction of a promising PS due to their ease of preparation and also their distinctive characteristics such as pH-sensitivity and biocompatibility.[51,52] In principle, these polymers can be disintegrated into smaller and non-toxic molecules *via* biodegradation of the ester bonds. In our previous reports, PBAEs were utilized as pH-responsive drug carriers for an anticancer drug[53] and antibiotics.[54]

Herein, we develop a PBAE-based, water-dispersible, biodegradable and biocompatible polymeric PS for effective PDT and imaging. PBAEs were designed to carry fluorescent groups, namely aza-BODIPY, and poly(ethylene glycol) segments in the polymer backbone through aza-Michael addition-based poly-condensation polymerization. PDT based anticancer and imaging potential of the polymer was demonstrated on brain tumor (U87-MG) and cervical cancer (HeLa) cell lines that overexpress FA receptors.

Experimental

Materials

Poly(ethylene glycol)diacrylate (PEGDA, M_n: 700 g mol^{-1}) (Sigma Aldrich), 5-amino-1-pentanol (AP) (95%, Sigma Aldrich), acetophenone (Aldrich), triethylamine (Et_3N) (Sigma Aldrich), magnesium sulfate (anhydrous) ($MgSO_4$) (Carlo Erba), acryloyl chloride (97%, Aldrich), *N*-hydroxysuccinimide (NHS) (Acros Organics), hydrochloric acid (HCl) (37%, Honeywell Fluka), sodium bicarbonate ($NaHCO_3$) (Merck), potassium hydroxide (KOH) (Merck), ammonium acetate (Supelco), nitromethane (Merck), *N*,*N*-diisopropylethylamine (DIEA) (Sigma Aldrich), boron trifluoride diethyl etherate ($BF_3{\cdot}OEt_2$) (Sigma Aldrich), triethylamine (Sigma Aldrich), folic acid (Sigma Aldrich), *N*,*N*′-dicyclohexylcarbodiimide (DCC) (Acros Organics), 2,6-di-*tert*-butyl-4-methylphenol 99% (BHT) (Acros Organics), ethylenediamine (Sigma Aldrich) and all other chemicals were obtained from commercial suppliers and used without further purification unless otherwise specified.

Synthesis of aza-BODIPY diacrylate (aza-BOD-DA)

Dihyroxyl functional aza-BODIPY (aza-BOD-OH) (100 mg, 1.89 × 10^{-4} mol, 1 eq.) was placed in a 2-neck flask and dissolved in 6 mL of tetrahydrofuran (THF), and triethylamine (264 μL, 1.89 × 10^{-3} mol, 10 eq.) was added to this solution under a nitrogen atmosphere. The reaction mixture was cooled down in an ice bath and a solution of acryloyl chloride (304 μL, 3.78 × 10^{-3} mol, 20 eq.) in 4 mL of THF was added dropwise. After 30 minutes of stirring at 0 °C, the reaction mixture was allowed to warm to room temperature and stirred overnight. The progression of the reaction was followed with thin layer chromato-

graphy (TLC), and THF was removed after completion of the reaction. The crude product was dissolved in ethyl acetate (120 mL) and washed with saturated sodium bicarbonate ($NaHCO_3$) (40 mL) solution and water (30 mL), sequentially. The organic layers were collected and dried over magnesium sulfate ($MgSO_4$), and the solvent was evaporated on a rotary evaporator. The resulting dark green colored aza-BOD-DA was dried under high vacuum (Scheme S2†) (yield: 95%).

^{1}H-NMR (500 MHz, $CDCl_3$) δ 8.10 (d, 4H), 8.05 (m, 4H), 7.50 (dd, J = 6.6, 3.6 Hz, 6H), 7.27 (d, 4H), 7.04 (s, 2H), 6.69–6.66 (dd, J = 17.4, 2.7 Hz, 2H), 6.41–6.35 (dd, 2H), 6.10–6.07 (dd, 2H). FT-IR: 3060 cm^{-1} (–CH═), 2925–2857 cm^{-1} (–C–H), 1735 cm^{-1} (–C(═O)–O–), 1600 cm^{-1} (–C═C–), 1478 and 1450 cm^{-1} (–B–N–, –C═C– or –C═N–), 1101 cm^{-1} (–C–O–), 1090 cm^{-1} (–B–F).

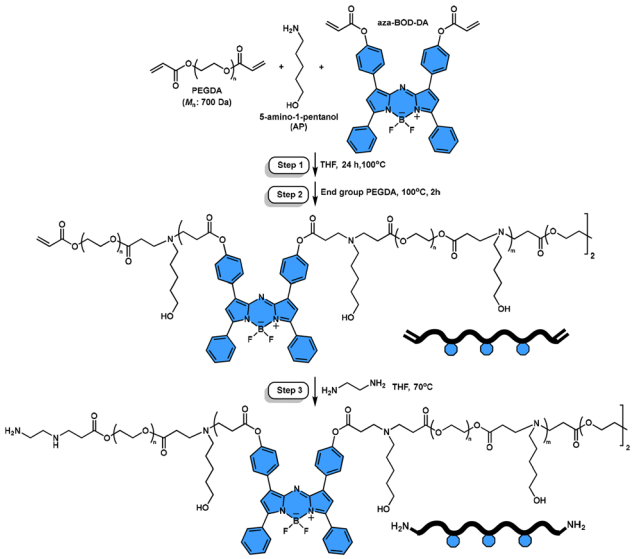

Scheme 1 One-pot synthesis of amine end-functionalized water soluble PBAEs.

One-pot synthesis of amine end-functionalized hydrophilic PBAE containing aza-BODIPY

Amine end-functionalized water soluble PBAEs were synthesized by a one-pot three-step approach, according to previously reported procedures with some modifications (Scheme 1).[55,56] Briefly, 1.0 g of PEGDA (M_n: 700 g mol^{-1}) (1.43 × 10^{-3} mol, 0.95 eq.) and 155 mg of 5-amino-1-pentanol (AP) (1.50 × 10^{-3} mol, 1.00 eq.) were dissolved in 1 mL of dry THF in an amber vial equipped with a magnetic stirrer. Then, a solution of aza-BOD-DA (48 mg, 7.53 × 10^{-5} mol, 0.05 eq., 5 mol%) in 1.5 mL of dry THF was added to the reaction mixture. Finally, 7 mg of BHT was added to this solution to prevent any possible free radical polymerization, and the vial was sealed off with a Teflon lid. The aza-Michael addition-based poly-condensation was conducted at 100 °C for 24 hours. Afterwards, 100 mg of PEGDA (1.43 × 10^{-4} mol, 0.10 eq.) was added, and the reaction was continued for further 2 hours for the complete conversion of end groups to acrylates (acr-wPBAE5%). Subsequently, the temperature was lowered to 70 °C and 29 μL of ethylenediamine (EDA) (4.34 × 10^{-4} mol, 0.29 eq.) in 10 mL of dry THF was added to the vial for amine end capping. The reaction was performed for various time periods (1, 3 and 5 h) for optimization of the end-capping process (the suitable time for amine end-capping was determined to be 5 h according to Fig. 1). Each time the resulting reaction mixture was cooled down to room temperature. The

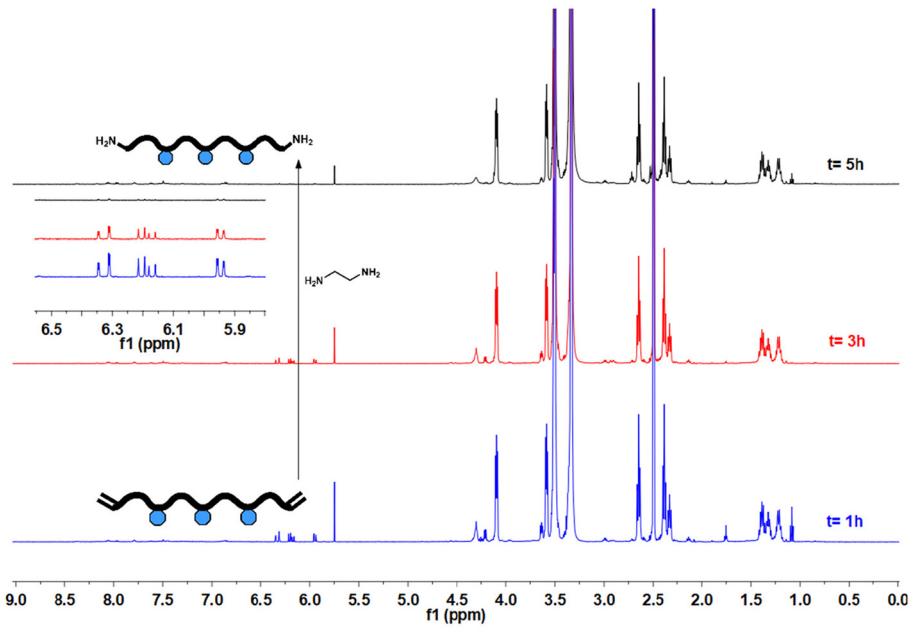

Fig. 1 ^{1}H-NMR spectra of the PBAEs (acr-wPBAE5%) treated with EDA for various periods of time (1, 3 and 5 hours) (DMSO-d_6).

excess THF was evaporated, and the polymer was precipitated in 80 mL of cold diethyl ether. The solvent was decanted, and the remaining polymer was dissolved in 1.5 mL of THF again and reprecipitated in 25 mL of cold ether twice. After centrifugation at 4000 rpm for 3 minutes, the amine end-functionalized PBAE was collected and dried under high vacuum (amino-wPBAE5%; 0.99 g; yield: 76%). Similarly, PBAEs containing 10% aza-BOD-DA were also synthesized (yield: 74%).

End-group transformation of amino PBAEs to folic acid

500 mg of amine end-functionalized PBAE (amine-wPBAE5%) was dissolved in 7 mL of DMSO, and 53.8 mg of the succinimidyl ester of folic acid (FA-NHS) (1×10^{-4} mol) in DMSO (2.5 mL) was added to the reaction solution. The flask was sealed off and the reaction solution was stirred at room temperature for 2 hours in the dark. Then, the reaction solution was precipitated into cold THF (20 mL) and centrifuged (8 minutes at 4000 rpm) to remove the unreacted FA-NHS. The supernatant was concentrated by evaporating excess THF and precipitated in 100 mL of ice-cold diethyl ether. The precipitate was redissolved in a minimal amount of THF and precipitated in 35 mL of cold diethyl ether again. The FA end-functionalized PBAE (FA-wPBAE5%) was obtained after drying under high vacuum (Scheme 2) (recovery >90%).

Singlet oxygen quantum yield (ϕ_Δ)

The singlet oxygen ($^1O_2$) quantum yield (ϕ_Δ) of aza-BODIPY-containing PBAEs is an important parameter for PDT. ϕ_Δ values of aza-BOD-OH and aza-BODIPY containing PBAEs were determined in ethanol using methylene blue (MB) as the standard (ϕ_Δ = 0.52).[57–59] Briefly, air saturated ethanol was prepared by bubbling air through ethanol for 15 min. Solutions of the $^1O_2$ scavenger, 1,3-diphenylisobenzofuran (DPBF), and the PS (MB, aza-BOD-OH or the polymer) were prepared separately in air saturated ethanol. Suitable amounts of these stock solutions were mixed to give a reaction solution with the absorbance values of DPBF and the PS being around 1.3 and 0.3, respectively. The solution in a quartz cuvette was irradiated with a red laser (CNI laser, model no: FC-680-2W; $\lambda \approx 680$ nm; I = 82 mW cm^{-2}) for specified time intervals, and the UV-Vis spectrum was recorded after each irradiation. The slope of the absorbance maximum of DPBF at 414 nm against time was determined for each sample. The ϕ_Δ values were calculated according to eqn (1):

$$\phi_{\Delta(\text{aza})} = \phi_{\Delta(\text{MB})} \times \frac{S_{(\text{aza})}}{S_{(\text{MB})}} \times \frac{F_{(\text{MB})}}{F_{(\text{aza})}} \quad (1)$$

where subscripts "aza" and "MB" refer to aza-BOD-OH or the polymers and MB, respectively. S is the slope of change in absorbance of DPBF at 414 nm against the irradiation time, and F represents the absorption correction factor ($F = 1 - 10^{-\text{O.D.}}$; O.D. is the optical density of the samples at the irradiation wavelength).

Fluorescence quantum yield (ϕ_F)

The fluorescence quantum yields (ϕ_F) of aza-BOD-OH and the polymers were determined using an optically matching solution of MB as the standard.[60,61] ϕ_F values of the polymers were determined in aqueous media, while the ϕ_F of aza-BOD-OH was determined in ethanol. Briefly, solutions of the PS (aza-BOD-OH or the PBAEs with aza-BODIPY groups) and the standard PS (MB) at three different concentrations were prepared (the absorbance values of the solutions around 650 nm were kept below 0.500). Then, fluorescence (excitation at 650 nm) and UV-Vis spectra of all samples were recorded.

The fluorescence quantum yield of the PS was calculated according to eqn (2):

$$\phi_{F(\text{aza})} = \phi_{F(\text{MB})} \times \frac{I_{(\text{MB})}}{I_{(\text{aza})}} \times \left[\frac{n_{(\text{MB})}}{n_{(\text{aza})}}\right]^2 \quad (2)$$

where ϕ_F is the fluorescence quantum yield, I is the slope of absorbance at the excitation wavelength (624 nm) *versus* the area under the fluorescence emission curve plot for each dye, and n is the refractive index of the solvents used. Subscripts "aza" and "MB" refer to aza-BOD-OH or the polymers and MB,

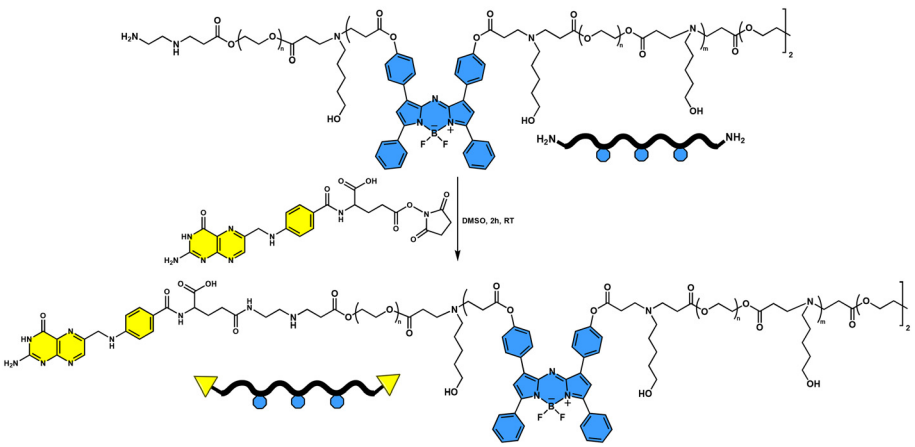

Scheme 2 End-group transformation of PBAEs with the succinimidyl ester of folic acid (FA-NHS).

respectively. The ϕ_F of MB is taken to be 0.04 in ethanol and 0.22 in water, as reported previously.[60,61]

Cell culture studies

Brain cancer cells (including U87-MG)[40] and human cervical cancer cells (HeLa)[43] were selected to show the imaging and anticancer potential of the fluorescent polymers, since HeLa cells and brain tissues carry excess FA receptors. U87-MG glioma and HeLa cervical tumor cells as well as non-cancerous HUVECs were obtained from the American Type Culture Collection (ATCC, USA). The cell lines were grown in Dulbecco's modified Eagle's medium (DMEM) (Wisent, #319-005CL) supplemented with 1% antibiotic–antimycotic (Wisent, #450-115EL) and 10% fetal bovine serum (ThermoFisher, #10500064). All cells were incubated in a humidified air incubator (5% CO_2) at 37 °C. In cell culture studies, cells were seeded at a maximum of 10% density of the wells and assays were done at a maximum of 80% confluency. The study was conducted *via* generating various cell groups by treatment of cells with either FA-wPBAE10% or FA-wPBAE5% polymers and with or without exposure to red LED light (λ = 630–700 nm wavelength, I = 2.4 mW cm^{-2}) for different periods of time. All cell culture experiments were carried out in triplicate and repeated at least two times; therefore, n = 6 for each experiment group.

Cellular uptake assay

U87-MG glioma cells and non-cancerous HUVECs were seeded on a 6-well plate (25×10^4 cells per well) and incubated at 37 °C with 5% CO_2 for 24 h. The cells were subjected to FA-wPBAE10% and FA-wPBAE5% (0.5 mg mL^{-1}) for 1 h. The cells were washed three times with 0.1% PBS. Fluorescence microscopy (Leica DM2500) was used to visualize and five different photographs of each group were taken. The excitation wavelength was 515–560 nm for each molecule. The cellular uptake was analyzed by counting the unstained and polymer containing cells on photographs. The percent cellular uptake was calculated as the ratio of all counted cells to cells with positive staining.

Cell viability assay

Cell proliferation and viability were measured using 3-(4,5-dimethylthiazol-2-yl)-2,5-diphenyl-2*H*-tetrazolium bromide (MTT) (US Biological, #258093) assay. U87-MG, HUVEC and HeLa cells were used to test the effects of FA-wPBAE10% and FA-wPBAE5% polymers on cell viability. 10×10^3 cells per well were seeded into each well of a 96-well plate, and the next day, the cells were treated with either FA-wPBAE10% or FA-wPBAE5% at concentrations ranging from 1 to 0.08 mg mL^{-1}. After overnight incubation at 37 °C with 5% CO_2, the plates were either incubated directly without exposure to red light or exposed to red light for durations of 30 and 60 minutes. Cells were incubated at 37 °C with 5% CO_2 for 24 h. After incubation, 10 μL of MTT solution (5 mg mL^{-1} in PBS) was added to each well and incubated for 2.5 h at 37 °C. 0.1 M HCl and 10% SDS solubilization buffer were added to dissolve the formazan crystals and incubated for 15 min at 37 °C. The absorbance was measured at 570 nm using a Thermo Varioskan Multimode Reader.

Reactive oxygen species (ROS) assay

Cellular reactive oxygen species (ROS) accumulation was assessed by flow cytometry with the fluorescent dye 2′,7′-dichlorodihydrofluorescein diacetate (DCFH-DA, Sigma-Aldrich). U87-MG and HeLa cells were seeded in 6-well plates and incubated at 37 °C with 5% CO_2 for 24 hours. Then the cells were treated in duplicate with either FA-wPBAE10% (0.1 mg mL^{-1}) or FA-wPBAE5% (0.3 mg mL^{-1}) and incubated at 37 °C with 5% CO_2 overnight. The plates were either incubated directly or exposed to red light for durations of 30 and 60 minutes. Following that, the cells were washed three times with 1× PBS. Subsequently, the cells were incubated in the dark at 37 °C with 10 μM DCFH-DA for 30 minutes. The cells were then washed three times with 1× PBS, trypsinized, and centrifuged at 500*g* for 10 minutes. The supernatant was removed, and the pellet was dissolved in 300 μL of 1× PBS. Flow cytometry (NovoCyte, ACEA Biosciences Inc., CA, USA) was used to analyze the excitation at 480 nm and emission at 530 nm.

Colony formation assay

The assay was performed in 6-well plates. HeLa cells were seeded at a density of 500 cells per well and 2 mL of the medium was added to each well. The next day, cells were treated in duplicate with either FA-wPBAE10% (0.1 mg mL^{-1}) or FA-wPBAE5% (0.3 mg mL^{-1}) and incubated at 37 °C with 5% CO_2 overnight. Plates were either incubated directly or exposed to red light for 30 and 60 minutes. On days 10–12, cells were washed twice with 1× PBS and fixed with ice-cold methanol for 5 min. 1% aqueous crystal violet solution (#V5265-250mL, Sigma-Aldrich, St Louis, MO, USA) was diluted with 1× PBS to 0.5% and added to the cells. Cells were incubated for 30 min at room temperature. Crystal violet was removed, and cells were washed under tap water and left to dry. Wells were scanned, and images were analyzed using Adobe Photoshop CC (Version 14.0) (San Jose, CA, USA).

Cell invasion assay

An xCELLigence RTCA DP system (Agilent, USA) was used to measure cell invasion. In order to assess the invasion capacity of the cells, RTCA CIM plates (Agilent, #5,665,817,001, USA) were used. Briefly, the upper chamber of the CIM plate was coated with 20 μL of diluted matrigel and incubated at 37 °C for 4 h. 160 μL of a medium supplemented with FBS was placed in the wells of the lower chamber. The assembled plate was put back into the incubator for an hour. 50 μL of the medium without FBS was distributed to the wells and background measurement was performed. U87-MG cells were seeded in 100 μL of the medium without FBS and with FA-wPBAE10% (0.1 mg mL^{-1}) or FA-wPBAE5% (0.3 mg mL^{-1}), and the plates were incubated in the cell culture hood for 30 min. Following the incubation, the plates were put back in the slot,

and after overnight incubation, the plates were either incubated directly or exposed to red light for a period of 30 minutes. The cell index was measured every 15 min for 48 h.

Instrumentation

An Agilent NMR system VNMRS 500 spectrometer was used for ^{1}H-NMR analysis at room temperature in deuterated solvents with $Si(CH_3)_4$ as the internal standard. UV-Vis analyses were performed on a Peak Instruments C-7000UV spectrophotometer with a 1 cm path length cuvette. Fluorescence measurements were performed in a quartz cell with 1 cm path length on an Agilent Cary Eclipse fluorescence spectrophotometer device at room temperature. During the fluorescence measurements, the excitation wavelength was set at 650 nm; the slit width was adjusted to be constant at 10 nm (excitation)/10 nm (emission) for the polymers and at 5 nm (excitation)/5 nm (emission) for small molecules; also, the device voltage was adjusted to 600 V. Fourier transform infrared (FT-IR) measurements were performed using an Agilent Technologies Cary 630 FT-IR instrument in the 4000–400 cm^{-1} scanning range and 32 scan numbers. A Tosoh EcoSEC dual detection (RI and UV) GPC system coupled with an external Wyatt Technologies Dawn Heleos-II multi-angle light scattering (MALS) detector and a Wyatt Technologies DynaPro NanoStar dynamic light scattering (DLS) detector was used for the determination of molecular masses of the polymers. DMF was used as the eluent at a flow rate of 0.5 mL min^{-1} at 45 °C. The columns set were one Tosoh TSKgel G5000HHR column (7.8 × 300 mm), one Tosoh TSKgel G3000HHR column (7.8 × 300 mm), one Tosoh TSKgel SuperH-RC reference column for EcoSEC and one Tosoh TSKgel HHR-H guard column (6 × 40 mm). Absolute molecular weights and molecular weight distributions were calculated using the Astra 7.1.2 software package. Dynamic light scattering (DLS) (Malvern Zetasizer Nano ZS, Malvern Instruments, UK) measurements were performed to determine the average size and size distribution of the particles. For morphology analysis, highly diluted polymers in water were dropped on a carbon film-coated Cu grid and left to dry. Samples were imaged on a Thermo Scientific Quattro ESEM scanning electron microscope (30 kV) equipped with a transmission electron detector (STEM) under high vacuum from a working distance of 7.6 mm, and the digital images of the samples were captured.

Results and discussion

Synthesis of the aza-BODIPY monomer (aza-DOD-DA)

The fluorescent monomer, aza-DOD-DA, was obtained through a typical synthesis of dihydroxy aza-BODIPY (aza-BOD-OH, Scheme S1†) followed by modification of the hydroxyl groups with acryloyl chloride (Scheme S2†).[62] Structures of the precursor molecules and aza-BOD-OH were analyzed and confirmed by FT-IR, NMR, UV-VIS and fluorescence spectroscopy (Fig. S1–S7†). Most importantly, a bathochromic shift of the absorption maximum from 612 nm to 674 nm supported the successful incorporation of $-BF_2-$ into the aza-dipyrromethene yielding aza-BOD-OH, as shown in Fig. S7.†[63] In addition, aza-BOD-OH showed a strong emission band at 708 nm, whereas the aza-dipyrromethene precursor did not show any fluorescence.[64] Chemical structures of the aza-BOD-OH and aza-DOD-DA were confirmed by NMR and FT-IR spectroscopy. The NMR spectra of aza-BOD-OH (Fig. S5†) and aza-BOD-DA (Fig. S8†) contain all characteristic aromatic proton peaks in the range of 6.85–8.10 ppm. After modification of aza-BOD-OH with acryloyl chloride, the phenolic proton peak at 10.15 ppm completely disappeared; new peaks attributed to three protons of the acrylate groups appeared at 6.68, 6.38 and 6.08 ppm. The ^{13}C-NMR spectrum of aza-BOD-DA (Fig. S9†) was also consistent with the proposed structure. Furthermore, FT-IR results supported the successful modification of aza-BOD-OH to aza-BOD-DA. The disappearance of the hydroxyl bands around 3500 cm^{-1} and the emergence of a strong carbonyl band at 1730 cm^{-1} in the FT-IR spectrum of aza-BOD-DA (Fig. S10B†) confirmed the presence of the acrylate groups in the structure.

Synthesis of water soluble fluorescent PBAEs with folic acid end groups

The water-soluble polymeric PSs based on PBAEs with aza-BODIPY groups in the main chain were synthesized through conventional aza-Michael addition-based poly-condensation polymerization.[55,56,65] 5-Amino-1-pentanol (AP) was preferred as the amine monomer; PEGDA and aza-BOD-DA were chosen as water soluble and fluorescent acrylate monomers, respectively. The polymers were obtained using a one-pot three-step synthetic approach involving (1) polymerization, (2) end-capping with acrylates and (3) end-capping with amines (Scheme 1).

First, the polymerization conditions were optimized with acrylate end-functionalized polymers which were obtained by performing only the first two steps of the three-step synthetic approach. The polymers were obtained with acrylate end groups in yields of 64–81% and with molecular mass around 5000–7700 g mol^{-1}. The acrylate end-capped polymers were also used for the approval of the aza-BODIPY content. The aza-BODIPY contents of acr-wPBAE10%, acr-wPBAE5% and acr-wPBAE1% were determined to be 8.2%, 4.9%, and 2.4%, respectively, which were in compliance with the feed ratio (see Table 1). The reaction conditions of acr-wPBAE5% were chosen for optimization of amine end group transformation. Excess amounts of amine (*i.e.* EDA) or extended reaction times may cause degradation of PBAEs during the amine end-capping process.[66] Therefore, the reaction duration and the amount of the amine (EDA) were optimized. The appropriate amount of amine was determined to be 0.29 molar equivalents of the overall acrylate monomers. Higher amounts probably led to degradation of the polymer, because aqueous solutions of the polymers exhibited no or very weak fluorescence whereas strong fluorescence was observed for polymers in THF (the results are not given). The degradation might yield small polymer fragments with a highly hydrophobic aza-BODIPY

Table 1 The PBAEs synthesized

Polymer	Monomer feed ratio [AP] : [PEGDA] : [aza-BOD-DA]	End-group	Yield[a] (%)	$M_{n,NMR}$ (g mol^{-1}) (DP)[b]	Aza-BOD-DA incorporation ratio[d] (%)	M_w[g] (g mol^{-1})	PDI[g]	$\lambda_{abs.}$[h] (nm)	$\lambda_{em.}$[i] (nm)
Acr-wPBAE10%	1.0 : 0.90 : 0.10	Acrylate	64	5020 (6.3)	8.2	8.7×10^3	1.69	682	706
Acr-wPBAE5%	1.0 : 0.95 : 0.05	Acrylate	81	5440 (6.8)	4.9	2.0×10^4	2.20	674	709
Acr-wPBAE1%	1.0 : 0.99 : 0.01	Acrylate	75	7710 (9.6)	2.4[e]	6.0×10^4	2.39	671	708
Amine-wPBAE10%	1.0 : 0.90 : 0.10	Amine	74	N.D.[c]	7.2	2.5×10^4	3.12	677	707
Amine-wPBAE5%	1.0 : 0.95 : 0.05	Amine	76	N.D.[c]	3.6	4.6×10^4	3.44	669	706
FA-wPBAE10%	1.0 : 0.90 : 0.10	FA	—	N.D.[c]	14.6[f]	4.7×10^4	5.43	674	709
FA-wPBAE5%	1.0 : 0.95 : 0.05	FA	—	N.D.[c]	7.9[f]	8.5×10^4	6.48	671	710

[a] Yields were determined gravimetrically. [b] Molecular masses of the polymers and degrees of polymerization (DP) were calculated using end group analysis based on the peaks belonging to the protons of the end acrylates and AP's methylene protons in the NMR spectrum. [c] The values could not be determined from NMR spectra. [d] Molar incorporation ratio of aza-BOD-DA was calculated from the peaks belonging to aza-BODIPY and peaks of methylene groups of AP in the NMR spectrum. [e] Since the sizes of the peaks in the NMR spectrum were quite small, the calculated value may result in a relatively high error. [f] These values were higher than the expected values since the baseline in the NMR spectra of FA terminated polymers was not as smooth as that of the amine terminated polymers. [g] The molecular masses and polydispersity index (PDI) were determined on a GPC device with DMF as the eluent. [h] The wavelengths of maximum absorbance were determined from UV-Vis spectra recorded in water. [i] The wavelengths of maximum emission were determined from fluorescence spectra recorded in water.

group which were not soluble in water but soluble in THF. In the optimization of the time period of amine end-capping, 5-hour treatment with the amine resulted in complete transformation as evaluated by NMR spectroscopy (Fig. 1). Therefore, these optimal conditions were employed in the synthesis of the subsequent polymers.

After optimization of the polymerization conditions, two different polymers were prepared with two different feed ratios of aza-BOD-DA (5 and 10 mol% with respect to acrylate) using the one-pot approach (Scheme 1). Excess PEGDA (0.10 eq.) and EDA (0.29 eq.) were sequentially added to the reaction medium for the complete conversion of end groups to acrylate and amine, correspondingly, after the polymerization step. The chemical structures of the polymers were confirmed by NMR spectroscopy. The ^{1}H-NMR spectra of amine end-functionalized polymers (amine-wPBAE10% and amine-wPBAE5%) are depicted in Fig. S14 and S15.† The strong peak at 3.66 ppm attributed to methylene protons of the PEG chain, the peaks of methylene proton neighbouring the tertiary amine at 2.77 ppm, and the proton peaks of AP at 1.32–1.61 and 3.70 ppm confirmed the accomplishment of the Michael addition-based poly-condensation. Most importantly, the appearance of typical aromatic peaks at 6.90–8.05 ppm verified the incorporation of the aza-BODIPY moieties (the incorporation ratios are given in Table 1). The absence of the acrylate proton peaks, which would appear at 5.80–6.40 ppm, was interpreted as the complete transformation of the acrylates to the amines.

In the next step, folic acid (FA) conjugation to the terminal amino group of the polymers was achieved using the succinimidyl ester of FA (FA-NHS) (Scheme 2) (see the ESI for synthesis and characterization of FA-NHS; Scheme S3, Fig. S11 and S12†). FT-IR spectra of both amine and FA end-functionalized polymers (Fig. S16†) exhibited bands of the main functionalities such as –OH (at 3466 cm^{-1}), –C–H (at 2933 and 2857 cm^{-1}), –C═O (at 1720 cm^{-1}) and –C–O–C– (at 1087 cm^{-1}) supporting the chemical structure of the polymers. For a comprehensive understanding of the transformation, NMR spectroscopy was employed. Comparative NMR spectra of acylate, amine and FA end-functionalized polymers (Fig. 2) verified the conjugation of the FA group. Specifically, the peaks at 6.62 ppm (peak d), 6.91 ppm (peak c) and 8.63 ppm (peak a) were assigned to the typical aromatic proton peaks of FA accurately, as indicated by the individual NMR spectra of FA-wPBAE10% (Fig. S17†) and FA-wPBAE5% (Fig. S18†).[67,68]

Physicochemical and photophysical properties

The effectiveness of PDT and bioimaging depends on the physicochemical and photophysical properties of the PS such as water solubility/dispersibility and absorption/emission in the NIR region. Therefore, such properties of the precursor molecules and the polymers were examined. Since the precursor molecules, aza-BOD-OH and aza-BOD-DA, were soluble in organic solvents, the UV-Vis and fluorescence spectra were recorded in THF (Fig. S20†). Both aza-BOD-OH and aza-BOD-DA showed typical absorbance bands with maxima at 669 nm and 655 nm and emission bands with maxima at 708 nm and 680 nm, respectively. The spectral performance in the NIR region (650–900 nm) is characteristic of aza-BODIPYs.[17,34,69] Moreover, their molar absorptivity coefficients (ε_{max}) were found to be 70 937 M^{-1} cm^{-1} (aza-BOD-OH) and 50 485 M^{-1} cm^{-1} (aza-BOD-DA). Such PSs exhibiting activity in the NIR region with high molar absorptivity coefficients are valuable for biomedical applications due to their enhanced tissue penetration.[34,70,71] However, these aza-BODIPYs were not soluble/dispersible in water due to their hydrophobic nature. This drawback was addressed by incorporating aza-BODIPY groups into the backbones of water-soluble PBAEs. The polymers in water showed a completely homogeneous and transparent appearance with a distinctive blue color of aza-BODIPY (Fig. 3A–C). Both DLS measurements and STEM images of the polymers (0.5 mg mL^{-1}) revealed that the polymers formed nanoparticles in an aqueous medium. The average particle sizes and PDIs of the samples obtained by

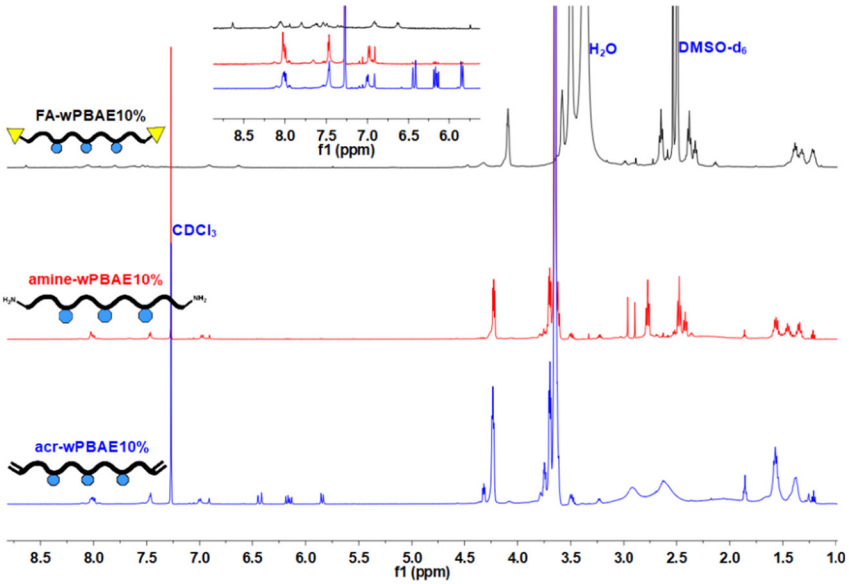

Fig. 2 ^{1}H-NMR spectra of acr-wPBAE10% ($CDCl_3$), amine-wPBAE10% ($CDCl_3$) and FA-wPBAE10% (DMSO-d_6).

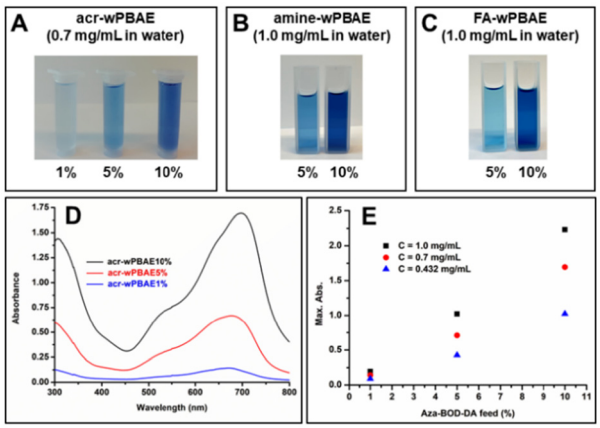

Fig. 3 Photographic images of acrylate (A), amine (B) and FA (C) end-functional PBAEs dispersed in water; UV-Vis spectra of acrylate end-functional PBAEs (0.7 mg/mL) (D); and the corresponding plot of aza-BOD-DA feed ratio and absorption maxima (E).

DLS are given in Table S1 and Fig. S19.† FA-wPBAE10% and FA-wPBAE5% had average sizes of 98.1 nm and 108.8 nm with a unimodal distribution, respectively (Fig. 4A–D). These polymers exhibited a globular morphology and sub-100 nm sizes as shown in the STEM images (Fig. 4E). Such nano-sized polymeric particles are highly demanded for passive targeting of tumor tissues *via* the EPR effect.[38]

As shown in Fig. 3, the blue color and homogeneous appearance supported successful incorporation of aza-BODIPY groups into the polymer chains. Increasing the feed ratio of aza-BOD-DA resulted in a darker color and stronger absorption bands in the UV-Vis spectra (Fig. 3D). This linear relationship between the aza-BOD-DA feed ratio and the absorption maxima (Fig. 3E) is also a good indicator of the efficient incorporation of aza-BODIPYs into the polymers. The incorporation ratio of aza-BOD-DA was quantitatively determined by both NMR (by mole) and UV-Vis (by mass) spectroscopy (Table 2). The aza-BOD-DA molar incorporation ratio was calculated from the proportion of typical aromatic peaks of aza-BODIPY at 6.90–8.05 ppm to peaks of methylene groups of 5-amino-1-pentanol at 1.20–1.40 ppm in the NMR spectrum. In addition, UV-Vis spectroscopy was employed to support the incorporation ratios determined by NMR spectroscopy. For this, the fraction of aza-BOD-DA (by mass) was calculated using the maximum absorbance values of the polymer solutions and the calibration curve of aza-BOD-DA in THF (Fig. S20F†). The incorporation ratios were determined to be 2.4% and 4.1% by mass for amine-wPBAE5% and amine-wPBAE10%, respectively. To compare the incorporation ratios obtained from NMR and UV-Vis spectroscopy, the incorporation efficiencies were calculated by determining the proportion of the feed ratio to the incorporation ratio (Table 2). The efficiencies were found in the range of 51–76% (by mass) by UV-Vis spectroscopy and were comparable with some of the molar incorporation efficiencies determined by NMR spectroscopy. However, values obtained from UV-Vis spectroscopy were deemed more reliable. Small peaks and an uneven baseline in NMR spectra may introduce a higher error margin, which was observed especially in acr-wPBAE1% and FA-wPBAE10%.

To get further insight into the biological applications, UV-Vis and fluorescence spectra of all PBAEs were recorded in aqueous media (Fig. S21–S24†). The maximum absorption wavelengths were found in the NIR region ranging from 669 nm to 696 nm. In all cases, the absorption spectra showed a linear concentration-dependent manner, as the concentration (mg mL^{-1}) against absorbance maxima exhibited a

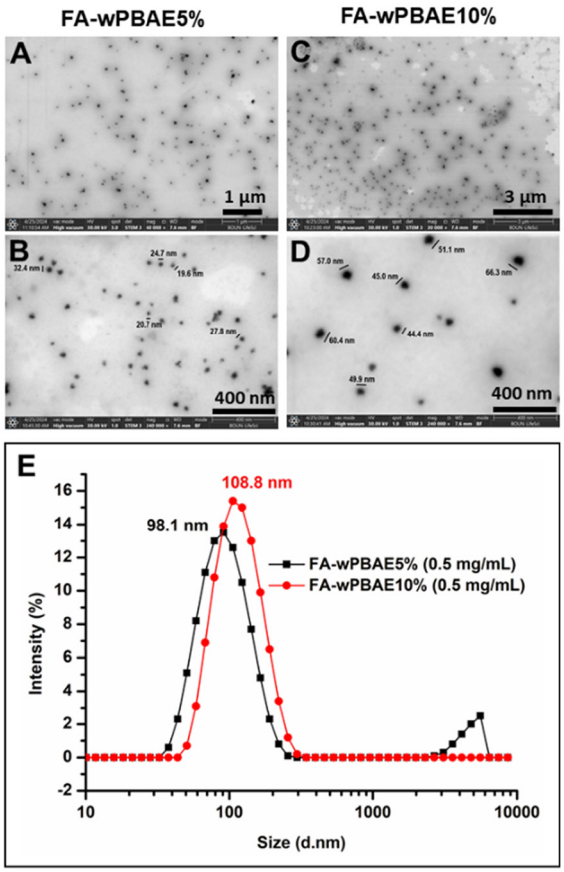

Fig. 4 STEM images of FA-wPBAE5% (A and B) and FA-wPBAE10% (C and D) and particle size distribution of these polymers in water determined with DLS (E).

linear fit with a decent coefficient of determination (R^2). On the other hand, the fluorescence intensities exhibited a completely different behavior regarding the concentrations. The emission maxima of the polymers in aqueous media initially increased and then decreased dramatically with increasing concentration (Fig. S25A†). This behaviour was attributed to aggregation induced quenching, which was also observed for previously reported aza-BODIPYs.[72–74] In addition, the maximum emission wavelengths shifted to longer wavelengths with increasing concentration or increasing aza-BODIPY content. For instance, the maximum emission wavelength of amine-wPBAE10% was found in the range of 702–759 nm for different concentrations (Fig. S25B†). This bathochromic shift with increasing aza-BODIPY content is caused by J-aggregation, as reported in previous studies.[72–74] Based on all these results, the suitable polymer concentration for imaging experiments was chosen to be 0.5 mg mL^{-1} which exhibited the highest fluorescence intensity and did not affect the cells.

Singlet oxygen quantum yield (ϕ_Δ) and fluorescence quantum yield (ϕ_F)

Singlet oxygen is considered to be the main cytotoxic agent in photodynamic therapy (PDT), and hence, singlet oxygen generation upon irradiation of PSs was monitored using the singlet oxygen quantum yield (ϕ_Δ). A common approach for determination of ϕ_Δ relies on tracking the absorbance (at 414 nm) of 1,3-diphenylisobenzofuran (DPBF), a singlet oxygen scavenger, upon irradiation of the PS.[58,59] Principally, the PS absorbs the light (around 650–670 nm) and produces singlet oxygen from molecular oxygen *via* intersystem crossing (ISC).[75] Subsequently, the reactive singlet oxygen ($^1O_2$) decomposes DPBF (Fig. S26A†) leading to a decrease in the absorbance of DPBF at 414 nm. In this study, singlet oxygen mediated photobleaching of DPBF in the presence of a reference PS, namely methylene blue (MB), the precursor molecule (aza-BOD-OH) and all polymers was monitored. Photobleaching of DPBF upon irradiation of MB and aza-BOD-OH in air saturated ethanol was exemplified and is shown in Fig. S26B and S26C.†

Table 2 Aza-BOD-DA incorporation efficiencies of PBAEs obtained from NMR and UV-Vis spectroscopy

	Aza-BOD-DA feed ratio		Aza-BOD-DA incorporation ratio		Incorporation efficiency	
Polymer	Mol% [a]	Mass% [b]	Mol% [c] (by NMR)	Mass% [f] (by UV-Vis)	Mol% [h] (by NMR)	Mass % [i] (by UV-Vis)
Acr-wPBAE10%	10.0	8.0	8.2	6.1	82	76
Acr-wPBAE5%	5.0	4.0	4.9	2.6	98	65
Acr-wPBAE1%	1.0	0.78	2.4[d]	0.42	>100	54
Amine-wPBAE10%	10.0	8.0	7.2	4.1	72	51
Amine-wPBAE5%	5.0	4.0	3.6	2.4	72	60
FA-wPBAE10%	10.0	8.0	14.6[e]	N.D.[g]	>100	N.D.[g]
FA-wPBAE5%	5.0	4.0	7.9[e]	N.D.[g]	>100	N.D.[g]

[a] Aza-BOD-DA feed ratios (by mole) were calculated with respect to the overall molar amount of diacrylate monomers utilized in the synthesis. [b] Aza-BOD-DA feed ratios (by mass) were calculated with respect to the overall mass of all monomers utilized in the synthesis. [c] Aza-BOD-DA incorporation ratios were determined from the ratio of peaks of the aza-BODIPY proton to peaks of methylene groups of 5-amino-1-pentanol in the NMR spectrum. [d] Since the sizes of the peaks in the NMR spectrum of Acr-wPBAE1% were quite small, the calculated value may result in a relatively high error. [e] These values were higher than the expected values since the baseline in the NMR spectra of FA terminated polymers was not as smooth as that of the amine terminated polymers. Therefore, the calculated values may have relatively high errors. [f] Aza-BOD-DA incorporation ratios (by mass) were calculated by taking the proportion of concentration of aza-BODIPY (obtained *via* UV-Vis spectroscopy) to the polymer concentration. [g] Since the polymers showed poor solubility in THF, these values could not be determined. [h] Molar incorporation efficiency was calculated by taking the proportion of the feed mole ratio to the incorporation mole ratio. [i] Incorporation efficiency (by mass) was calculated by taking the proportion of the feed mass ratio to the incorporation mass ratio.

Table 3 Singlet oxygen quantum yields (ϕ_Δ) and fluorescence quantum yields (ϕ_f) of aza-BOD-OH and the PBAEs

Polymer	Singlet oxygen quantum yield (ϕ_Δ)[a]	Fluorescence quantum yield (ϕ_f)[b]	$\lambda_{abs.}$ [b](nm)	$\lambda_{em.}$ [b] (nm)
Acr-wPBAE10%	0.030	0.0034	682	706
Acr-wPBAE5%	0.032	0.0074	674	709
Acr-wPBAE1%	0.035	0.0150	671	708
Amine-wPBAE10%	0.036	0.0042	677	707
Amine-wPBAE5%	0.045	0.0081	669	706
FA-wPBAE10%	0.034	0.0114	674	709
FA-wPBAE5%	0.026	0.0255	671	710
Aza-BOD-OH (in ethanol)	0.044	0.0225	663	712
MB (in water)	—	0.22 [60]	664	684
MB (in ethanol)	0.52 [57]	—	655	677

[a] Singlet oxygen quantum yields (ϕ_Δ) were determined in ethanol using MB as the reference PS. [b] Fluorescence quantum yields (ϕ_F), maximum absorbance wavelength ($\lambda_{abs.}$) and maximum emission wavelength ($\lambda_{em.}$) were determined in water using MB as the reference PS.

The absorbance values were plotted against the irradiation time to calculate the ϕ_Δ (Fig. S26D†). The ϕ_Δ of aza-BOD-OH was calculated to be 0.044 with respect to MB as the standard PS using eqn (1). This value is slightly higher than those of previously reported and structurally similar aza-BODIPYs (ϕ_Δ = 0.009–0.012).[76] The same approach was employed in the determination of ϕ_Δ values of the polymers which were found to be in the range of 0.026–0.045 in ethanol (Table 3). Even though the aza-BODIPY contents were quite low, the ϕ_Δ values of the PBAEs were comparable with the value of the precursor, aza-BOD-OH, and thus, they can be considered to be a promising PS for PDT.

Fluorescence quantum yields (ϕ_F) of the PBAEs and the precursor compound (aza-BOD-OH) were also determined. The ϕ_F of the precursor was found to be 0.0225 in ethanol, which is consistent with the literature values. Previous studies on aza-BODIPY conjugated with poly(ethylene glycol) (PEG-BODs) reported the ϕ_F to be 0.008–0.07 in methanol.[77] ϕ_F values of the PBAEs in an aqueous solution ranged between 0.0034 and 0.0255 with respect to the reference PS (ϕ_F of MB: 0.22). Although the values were relatively low, the polymers displayed strong radiation in the NIR region in cell culture experiments.

Biological assays

The cellular uptake assay aimed to assess the capacity of non-cancerous HUVECs and U87-MG glioma cells to take up the polymers into the intracellular environment. It was assessed by fluorescence imaging of both FA-wPBAE10% and FA-wPBAE5% polymers (Fig. 5A). The polymers showed a fluorescence intensity of 100% for both cell lines after 1 h treat-

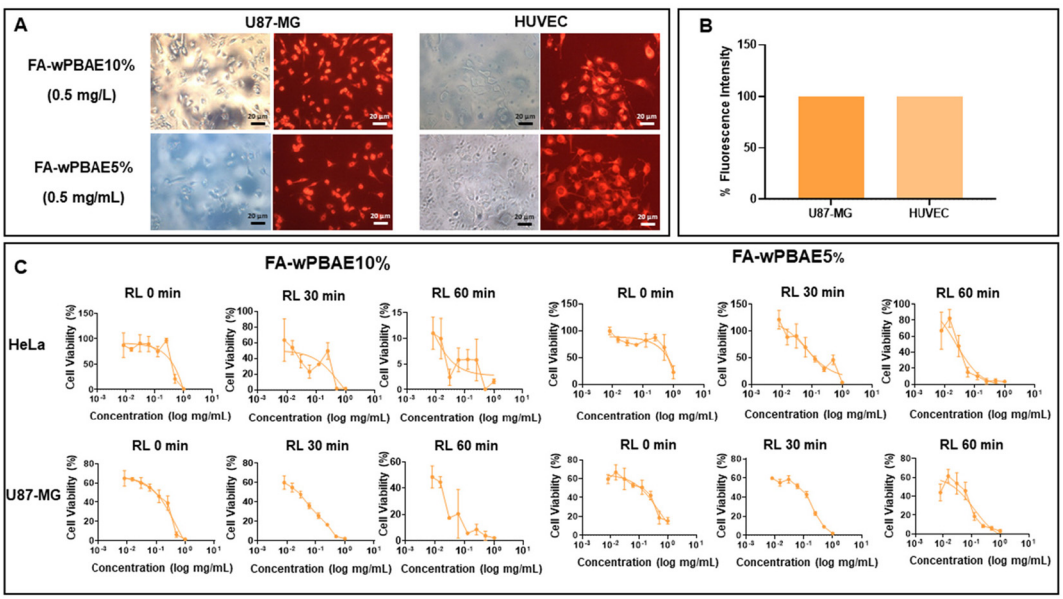

Fig. 5 The fluorescent PBAEs were taken up by cells and induced photocytotoxicity on cancerous cells. (A) Cellular uptake assay. Cells were treated with 0.5 mg mL^{-1} FA-wPBAE10% or FA-wPBAE5% and evaluated under a fluorescence microscope. Images are shown with 20× magnification. (B) Percentage fluorescence intensity of the cells treated with FA-wPBAE10%. (C) Cell proliferation assay of HeLa and U87-MG cells. Concentrations of both FA-wPBAE10% and FA-wPBAE5% range from 1 to 0.08 mg mL^{-1}. 0 minutes indicates no red-light exposure. 30 and 60 minutes indicate that cells were exposed to red light (λ = 630–700 nm) for 30 minutes in one group and 60 minutes in another group.

ment with 0.5 mg mL^{-1} concentration (Fig. 5B). The findings demonstrated that the polymers were able to effectively penetrate the cells within one hour and did not cause any toxic damage to the cells. This highly efficient cellular penetration can be attributed to the cationic nature of PBAEs at lower pH values (>6.5) and their favorable interaction with negatively charged cell surfaces.[52] FA groups of the polymers did not make a significant difference for cellular uptake in these cell culture experiments; however, these FA functionalities would be beneficial for overcoming the blood–brain barrier (BBB) since FA receptors are common receptors expressed on the BBB.[40] As a result, it is suggested that the designed polymer structure serves as a successful system for delivering the PS to specific targets without damaging the cells.

The purpose of the cell proliferation assay was to evaluate the anti-cancer effects of polymers on cancer cells. Cell proliferation after treatment of U87-MG and HeLa cells with the PBAEs and red-light exposure (λ = 630–700 nm) was compared. Dose-dependent anti-cancer activity of both polymers was observed. Red light exposure together with the polymers induced the aza-BODIPY moieties leading to singlet oxygen generation and a significant cell death in both polymers compared to the cells that were not exposed to red light. The half-maximal inhibitory concentration (IC_{50}) values were calculated and are shown in Fig. 6. Briefly, it can be concluded that the FA-wPBAE10% molecule showed better anti-cancer activity than FA-wPBAE5%. It was also observed that the polymers were more effective at relatively high concentrations in cells with no red-light exposure, whereas in cells exposed to red light for 30 and 60 minutes, they were effective at much lower concentrations (Fig. 5C and 6). Furthermore, FA-wPBAE5% was not toxic to non-cancerous HUVECs, while it showed significant anti-cancer activity against U87-MG and HeLa cells.

As intracellular ROS production due to PDT treatment is accompanied by cytotoxicity, ROS activity was measured in HeLa and U87-MG cells to evaluate photocytotoxicity. Both polymers induced ROS activity, and the longer the duration of the light exposure of both molecules, the higher the ROS

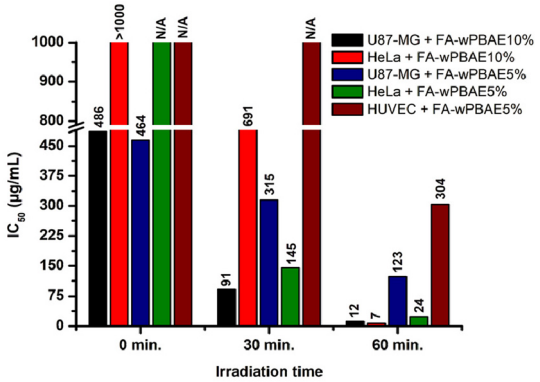

Fig. 6 Half maximal inhibitory concentration (IC_{50}) of FA-wPBAE10% or FA-wPBAE5% in photocytotoxicity assays (N/A refers to no toxic effects leading to the death of a minimum of 50% of cells).

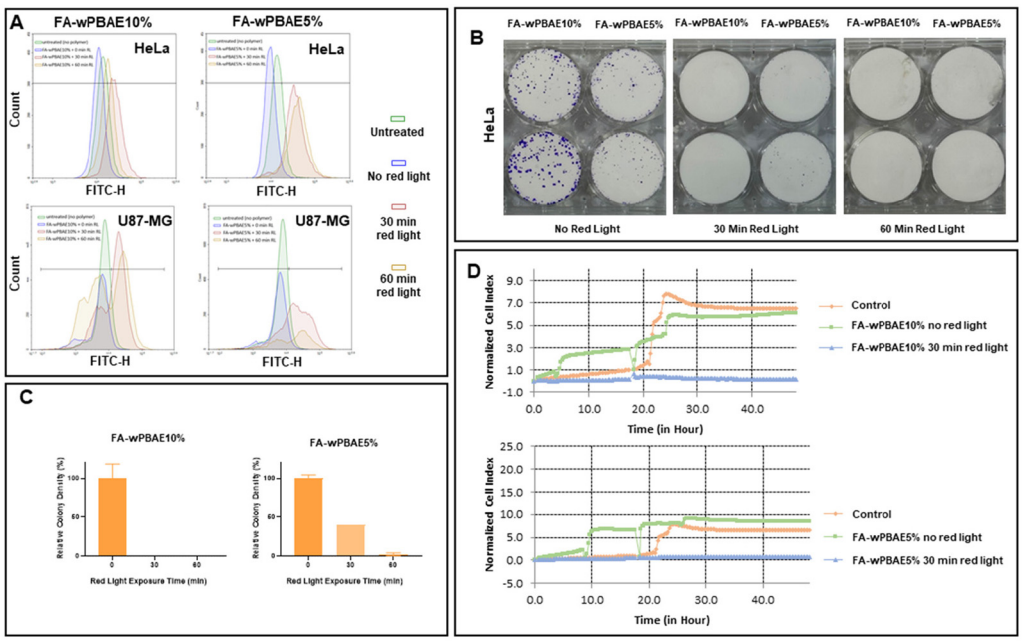

Fig. 7 The polymers promote ROS activity and reduce colony formation and invasion potential of cancerous cells upon irradiation. (A) Flow cytometric ROS activity analysis of HeLa and U87-MG cells by DCFH-DA staining, treated with FA-wPBAE10% and FA-wPBAE5% and red-light exposure. (B) Colony formation assay of HeLa cells. Images of HeLa colonies treated with FA-wPBAE10% (0.1 mg mL^{-1}) and FA-wPBAE5% (0.3 mg mL^{-1}) and exposed to red light on day 8. Cells were fixed with ice-cold methanol and stained with 0.5% crystal violet. (C) Percentage relative colony density normalized to the no red light control group. Colony density was determined as pixel counting using Adobe Photoshop. (D) Cell invasion assay of U87-MG cells. Cell index was measured every 15 min for 48 h on an X-Celligence system.

activity measured (Fig. 7A and Fig. S29†). Furthermore, prolonged light exposure caused a decrease in the number of cells along with an increase in ROS formation. The colony formation capability of cancer cells is proportional to the stemness potential of cancer cells because only cancer promoting stem cells generate colonies. It was observed that the number of colonies in the no red light exposed group increased; however, when the cells were exposed to red light, the number of cell colonies significantly reduced for both polymers (Fig. 7B). The FA-wPBAE10% molecule showed superior activity indicating almost no colony formation even in 30 minutes of red light exposure, while the FA-wPBAE5% molecule showed a significantly decreased number of colonies (Fig. 7C). The invasiveness potential of U87-MG cells after polymer treatment and red-light exposure was investigated using a real time impedance-based cell tracking system. Results revealed that both polymers target the cancer stem cells having colony formation potential.

Migration of cells to the growth factor attractant chamber is proportional to their cellular invasion and migration potential. Cells that underwent the polymer treatment without exposure to red light were used as controls along with cells that did not receive the polymer treatment, and they showed almost similar invasion. However, cells that are exposed to 30 minutes of red light together with both polymers showed no cellular invasion (Fig. 7D). Results indicated that both polymers reduce the invasion potential of cancer cells.

Conclusion

We have developed a biodegradable, highly water dispersible and fluorescent PBAE as an efficient PS for PDT and imaging. The PBAEs were specifically designed to have amine end groups through aza-Michael addition-based poly-condensation polymerization of acrylate functional aza-BODIPY, PEGDA and 5-amino-1-pentanol. The amine-end functionalized polymers were end-capped with folic acid to increase the cancer-cell-targeting efficiency of the PS. The polymers assembled into globular nano-sized particles, which is beneficial for passive tumor targeting. The fluorescent polymers demonstrated promising anti-cancer activities against U87-MG brain tumor cells and HeLa cervical tumor cells while showing no significant cytotoxicity on non-cancer cells. The mechanism of action for anticancer activity was found to be *via* singlet oxygen and ROS generation upon irradiation with red light. Moreover, the polymers with irradiation dramatically decreased colony formation and exhibited high potential in the prevention of cancer cell invasion. In addition, the polymers were found to be very effective in cancer cell imaging.

Author contributions

Seyma Sari: methodology, investigation, resources, data curation, and writing – original draft. Sena Ünver: formal analysis, investigation, and visualization. Timucin Avsar: formal analysis, methodology, funding acquisition, and writing – original draft. Şennur Özçelik: methodology, funding acquisition, writing – original draft, and writing – review and editing. Turker Kilic: methodology and resources. Muhammet Ubeydullah Kahveci: supervision, methodology, resources, conceptualization, project administration, funding acquisition, writing – original draft, and writing – review and editing.

Conflicts of interest

There are no conflicts to declare.

Acknowledgements

This work was financially supported by The Scientific and Technological Research Council of Turkey (TUBITAK, project # 120Z966) and the Istanbul Technical University Scientific Research Projects (ITU BAP, project # TDK-2022-44238). This work is dedicated to the memory of Professor Yusuf Yagci, a great contributor to the photochemistry of polymers. The authors would like to thank Prof. Bunyamin Karagoz for fluorescence spectroscopy measurements and Prof. Aydan Dag for GPC measurements.

References

1 H. Sung, J. Ferlay, R. L. Siegel, M. Laversanne, I. Soerjomataram, A. Jemal and F. Bray, *CA-Cancer J. Clin.*, 2021, **71**, 209–249.
2 D. Viswanath and Y. Y. Won, *ACS Biomater. Sci. Eng.*, 2022, **8**, 3644–3658.
3 J. C. S. Simões, S. Sarpaki, P. Papadimitroulas, B. Therrien and G. Loudos, *J. Med. Chem.*, 2020, **63**, 14119–14150.
4 T. J. Dougherty, *Photochem. Photobiol.*, 1993, **58**, 895–900.
5 A. Escudero, C. Carrillo-Carrión, M. C. Castillejos, E. Romero-Ben, C. Rosales-Barrios and N. Khiar, *Mater. Chem. Front.*, 2021, **5**, 3788–3812.
6 C.-G. Qian, Y.-L. Chen, P.-J. Feng, X.-Z. Xiao, M. Dong, J.-C. Yu, Q.-Y. Hu, Q.-D. Shen and Z. Gu, *Acta Pharmacol. Sin.*, 2017, **38**, 764–781.
7 S. S. Kelkar and T. M. Reineke, *Bioconjugate Chem.*, 2011, **22**, 1879–1903.
8 E. T. Sarcan, M. Silindir-Gunay and A. Y. Ozer, *Int. J. Pharm.*, 2018, **551**, 329–338.
9 P. Koralli, S. Tsikalakis, M. Goulielmaki, S. Arelaki, J. Müller, A. D. Nega, F. Herbst, C. R. Ball, V. G. Gregoriou, A. Dimitrakopoulou-Strauss, S. Wiemann and C. L. Chochos, *Mater. Chem. Front.*, 2021, **5**, 4950–4962.
10 Y.-Q. Huang, K.-L. Liu, H.-L. Ni, R. Zhang, X.-F. Liu, Q.-L. Fan, L.-H. Wang and W. Huang, *ACS Appl. Polym. Mater.*, 2022, **4**, 7739–7750.

11 T. J. Dougherty, C. J. Gomer, B. W. Henderson, G. Jori, D. Kessel, M. Korbelik, J. Moan and Q. Peng, *J. Natl. Cancer Inst.*, 1998, **90**, 889–905.
12 L. B. Josefsen and R. W. Boyle, *Theranostics*, 2012, **2**, 916–966.
13 R. R. Allison, G. H. Downie, R. Cuenca, X.-H. Hu, C. J. H. Childs and C. H. Sibata, *Photodiagn. Photodyn. Ther.*, 2004, **1**, 27–42.
14 L. Li and K. M. Huh, *Biomater. Res.*, 2014, **18**, 19.
15 T. C. Pham, V.-N. Nguyen, Y. Choi, S. Lee and J. Yoon, *Chem. Rev.*, 2021, **121**, 13454–13619.
16 X. Li, S. Lee and J. Yoon, *Chem. Soc. Rev.*, 2018, **47**, 1174–1188.
17 W. M. Gallagher, L. T. Allen, C. O'Shea, T. Kenna, M. Hall, A. Gorman, J. Killoran and D. F. O'Shea, *Br. J. Cancer*, 2005, **92**, 1702–1710.
18 X. Li, S. Kolemen, J. Yoon and E. U. Akkaya, *Adv. Funct. Mater.*, 2017, **27**, 1604053.
19 W. Zhao and E. M. Carreira, *Angew. Chem., Int. Ed.*, 2005, **44**, 1677–1679.
20 A. Kamkaew, S. H. Lim, H. B. Lee, L. V. Kiew, L. Y. Chung and K. Burgess, *Chem. Soc. Rev.*, 2013, **42**, 77–88.
21 G. Fan, L. Yang and Z. Chen, *Front. Chem. Sci. Eng.*, 2014, **8**, 405–417.
22 S. Cheung and D. F. O'Shea, *Nat. Commun.*, 2017, **8**, 1885.
23 E. Y. Xue, W.-J. Shi, W.-P. Fong and D. K. P. Ng, *J. Med. Chem.*, 2021, **64**, 15461–15476.
24 J. Pliquett, A. Dubois, C. Racoeur, N. Mabrouk, S. Amor, R. Lescure, A. Bettaïeb, B. Collin, C. Bernhard, F. Denat, P. S. Bellaye, C. Paul, E. Bodio and C. Goze, *Bioconjugate Chem.*, 2019, **30**, 1061–1066.
25 O. Florès, J. Pliquett, L. Abad Galan, R. Lescure, F. Denat, O. Maury, A. Pallier, P.-S. Bellaye, B. Collin, S. Même, C. S. Bonnet, E. Bodio and C. Goze, *Inorg. Chem.*, 2020, **59**, 1306–1314.
26 D. O. Frimannsson, M. Grossi, J. Murtagh, F. Paradisi and D. F. O'Shea, *J. Med. Chem.*, 2010, **53**, 7337–7343.
27 A. Kamkaew and K. Burgess, *Chem. Commun.*, 2015, **51**, 10664–10667.
28 H. C. Daly, G. Sampedro, C. Bon, D. Wu, G. Ismail, R. A. Cahill and D. F. O'Shea, *Eur. J. Med. Chem.*, 2017, **135**, 392–400.
29 S. Kampaengsri, K. Chansaenpak, G. Y. Yong, P. Hiranmartsuwan, B. Uengwanarat, R.-Y. Lai, P. Meemon, C. S. Kue and A. Kamkaew, *ACS Appl. Bio Mater.*, 2022, **5**, 4567–4577.
30 M. M. Kose, S. Onbulak, I. I. Yilmaz and A. Sanyal, *Macromolecules*, 2011, **44**, 2707–2714.
31 D. Dutta, R. R. Nair, S. Mangalath, S. A. Nair, J. Joseph, P. Gogoi and D. Ramaiah, *ACS Omega*, 2023, **8**, 26180–26190.
32 N. Adarsh, P. S. S. Babu, R. R. Avirah, M. Viji, S. A. Nair and D. Ramaiah, *J. Mater. Chem. B*, 2019, **7**, 2372–2377.
33 Y. Xu, T. Feng, T. Yang, H. Wei, H. Yang, G. Li, M. Zhao, S. Liu, W. Huang and Q. Zhao, *ACS Appl. Mater. Interfaces*, 2018, **10**, 16299–16307.
34 Z. Shi, X. Han, W. Hu, H. Bai, B. Peng, L. Ji, Q. Fan, L. Li and W. Huang, *Chem. Soc. Rev.*, 2020, **49**, 7533–7567.
35 G. Feng, Y. Fang, J. Liu, J. Geng, D. Ding and B. Liu, *Small*, 2017, **13**, 1602807.
36 L. Hu, Z. Chen, Y. Liu, B. Tian, T. Guo, R. Liu, C. Wang and L. Ying, *ACS Appl. Mater. Interfaces*, 2020, **12**, 57281–57289.
37 T. Senthilkumar and S. Wang, in *Conjugated Polymers for Biological and Biomedical Applications*, 2018, pp. 269–294, DOI: **10.1002/9783527342747.ch10**.
38 R. Sun, J. Xiang, Q. Zhou, Y. Piao, J. Tang, S. Shao, Z. Zhou, Y. H. Bae and Y. Shen, *Adv. Drug Delivery Rev.*, 2022, **191**, 114614.
39 D. Rosenblum, N. Joshi, W. Tao, J. M. Karp and D. Peer, *Nat. Commun.*, 2018, **9**, 1410.
40 E. McCord, S. Pawar, T. Koneru, K. Tatiparti, S. Sau and A. K. Iyer, *ACS Omega*, 2021, **6**, 4111–4118.
41 R. I. Pinhassi, Y. G. Assaraf, S. Farber, M. Stark, D. Ickowicz, S. Drori, A. J. Domb and Y. D. Livney, *Biomacromolecules*, 2010, **11**, 294–303.
42 F. Porta, G. E. M. Lamers, J. Morrhayim, A. Chatzopoulou, M. Schaaf, H. den Dulk, C. Backendorf, J. I. Zink and A. Kros, *Adv. Healthcare Mater.*, 2013, **2**, 281–286.
43 S. K. Sriraman, J. Pan, C. Sarisozen, E. Luther and V. Torchilin, *Mol. Pharm.*, 2016, **13**, 428–437.
44 C. Tian, J. Niu, X. Wei, Y. Xu, L. Zhang, Z. Cheng and X. Zhu, *Nanoscale*, 2018, **10**, 10277–10287.
45 C. Zhu, L. Liu, Q. Yang, F. Lv and S. Wang, *Chem. Rev.*, 2012, **112**, 4687–4735.
46 X. Feng, L. Liu, S. Wang and D. Zhu, *Chem. Soc. Rev.*, 2010, **39**, 2411–2419.
47 M. A. Campo, D. Gabriel, P. Kucera, R. Gurny and N. Lange, *Photochem. Photobiol.*, 2007, **83**, 958–965.
48 H. Huang, W. Xie, Q. Wan, L. Mao, D. Hu, H. Sun, X. Zhang and Y. Wei, *Adv. Sci.*, 2022, **9**, 2104101.
49 Q. Miao, C. Xie, X. Zhen, Y. Lyu, H. Duan, X. Liu, J. V. Jokerst and K. Pu, *Nat. Biotechnol.*, 2017, **35**, 1102–1110.
50 J. Liu, S. Wang, X. Cai, S. Zhou and B. Liu, *Chem. Commun.*, 2018, **54**, 2518–2521.
51 S. Iqbal, Y. Qu, Z. Dong, J. Zhao, A. R. Khan, S. Rehman and Z. Zhao, *Eur. Polym. J.*, 2020, **141**, 110097.
52 Y. Liu, Y. Li, D. Keskin and L. Shi, *Adv. Healthcare Mater.*, 2019, **8**, 1801359.
53 E. L. Sahkulubey Kahveci, M. U. Kahveci, A. Celebi, T. Avsar and S. Derman, *Biomacromolecules*, 2022, **23**, 4896–4908.
54 G. Bakirdogen, E. Selcuk, E. L. Sahkulubey Kahveci, T. Ozbek, S. Derman and M. U. Kahveci, *Int. J. Biol. Macromol.*, 2024, **258**, 129060.
55 A. A. Eltoukhy, D. J. Siegwart, C. A. Alabi, J. S. Rajan, R. Langer and D. G. Anderson, *Biomaterials*, 2012, **33**, 3594–3603.
56 A. Akinc, D. G. Anderson, D. M. Lynn and R. Langer, *Bioconjugate Chem.*, 2003, **14**, 979–988.
57 R. W. Redmond and J. N. Gamlin, *Photochem. Photobiol.*, 1999, **70**, 391–475.
58 S. Guo, L. Ma, J. Zhao, B. Küçüköz, A. Karatay, M. Hayvali, H. G. Yaglioglu and A. Elmali, *Chem. Sci.*, 2014, **5**, 489–500.

59 Q. Tang, W. Si, C. Huang, K. Ding, W. Huang, P. Chen, Q. Zhang and X. Dong, *J. Mater. Chem. B*, 2017, **5**, 1566–1573.
60 G. A. Shahinyan, A. Y. Amirbekyan and S. A. Markarian, *Spectrochim. Acta, Part A*, 2019, **217**, 170–175.
61 J. Olmsted, *J. Phys. Chem.*, 1979, **83**, 2581–2584.
62 J. Murtagh, D. O. Frimannsson and D. F. O'Shea, *Org. Lett.*, 2009, **11**, 5386–5389.
63 M. J. Hall, S. O. McDonnell, J. Killoran and D. F. O'Shea, *J. Org. Chem.*, 2005, **70**, 5571–5578.
64 Y. Ge and D. F. O'Shea, *Chem. Soc. Rev.*, 2016, **45**, 3846–3864.
65 S. Perni and P. Prokopovich, *Nanomedicine*, 2017, **13**, 539–548.
66 M. K. Kuenen, K. S. Reilly and R. A. Letteri, *ACS Macro Lett.*, 2023, **12**, 1416–1422.
67 H. Zhao and L. Y. L. Yung, *Int. J. Pharm.*, 2008, **349**, 256–268.
68 J. Qiao, P. Dong, X. Mu, L. Qi and R. Xiao, *Biosens. Bioelectron.*, 2016, **78**, 147–153.
69 Ş. Özçelik, A. G. Yurttaş, M. U. Kahveci, A. M. Sevim and A. Gül, *J. Mol. Struct.*, 2023, **1271**, 134019.
70 A. Gut, Ł. Łapok, D. Jamróz, A. Gorski, J. Solarski and M. Nowakowska, *New J. Chem.*, 2017, **41**, 12110–12122.
71 L. Huang, Z. Li, Y. Zhao, J. Yang, Y. Yang, A. I. Pendharkar, Y. Zhang, S. Kelmar, L. Chen, W. Wu, J. Zhao and G. Han, *Adv. Mater.*, 2017, **29**, 1604789.
72 Z. Chen and Z. Chen, *Org. Chem. Front.*, 2023, **10**, 2581–2602.
73 Y. Tian, D. Yin, Q. Cheng, H. Dang, C. Teng and L. Yan, *J. Mater. Chem. B*, 2022, **10**, 1650–1662.
74 K. Cai, J. Xie and D. Zhao, *J. Am. Chem. Soc.*, 2014, **136**, 28–31.
75 A. Gorman, J. Killoran, C. O'Shea, T. Kenna, W. M. Gallagher and D. F. O'Shea, *J. Am. Chem. Soc.*, 2004, **126**, 10619–10631.
76 N. Adarsh, R. R. Avirah and D. Ramaiah, *Org. Lett.*, 2010, **12**, 5720–5723.
77 X. He, H. Li, S. Liu, Y. Li, X. Lin, H. Zheng, Z. Zhou and D. Zeng, *ChemistrySelect*, 2022, **7**, e202103821.